Available online at www.sciencedirect.com
SCIENCE DIRECT®
Journal of Sound and Vibration 283 (2005) 341–368
JOURNAL OF SOUND AND VIBRATION
www.elsevier.com/locate/jsvi

Flexural damage index equations of a plate

Byeong Hwa Kim[a], Norris Stubbs[b], Taehyo Park[c,*]

[a]*Computational Solid & Structural Mechanics Laboratory, Department of Civil Engineering, Hanyang University, 17 Haengdang-dong, Seoul 133-791, Korea*
[b]*Department of Civil Engineering, MS 3136, Texas A&M University, College Station, TX 77843, USA*
[c]*Department of Civil Engineering, Hanyang University, 17 Haengdang-dong, Seoul 133-791, Korea*

Received 9 October 2003; received in revised form 17 March 2004; accepted 19 April 2004
Available online 21 November 2004

Abstract

A new nondestructive damage evaluation method is introduced. The method is able to detect, locate, and size structural damage in a plate-like structure using measured modal parameters of a structure. The solution procedure consists of two steps: First, the method requires constructing a set of flexural damage index equations that represent a rigorous mechanical relationship between damage and curvature of modal flexibility. Second, a *pseudo*-inverse solution to the resulting system of the over-determined equation nondestructively evaluates damage in a plate-like structure. This study confirms that there is a strong linear relationship between the curvature of flexibility of a structure and flexural damage. In consequence, the proposed method introduces a way to avoid the singularity problem and mode selection problem of the mode shape curvature method and damage index method.

1. Introduction

Due to a variety of hostile environments, the unexpected structural deterioration in existing structures is unavoidable. In order to monitor periodically the load carrying capacity of the structure, many nondestructive damage evaluation techniques have been proposed over last three decades. Among the vibration-based damage detection methods, the Mode Shape Curvature (MSC) method by Pandey et al. [1] and the Damage Index (DI) method by Stubbs et al. [2] have

*Corresponding author. Tel.: +82-2-2290-0321; fax: +82-2-2293-9977.
E-mail address: cepark@hanyang.ac.kr (T. Park).

0022-460X/$ - see front matter © 2004 Elsevier Ltd. All rights reserved.
doi:10.1016/j.jsv.2004.04.035

Nomenclature

$\boldsymbol{\alpha}$	the 12×1 vector for a plate, containing the coefficient of the polynomial state
$\beta^{e,f}$	the flexural damage index of the (e,f)th element of a plate
$\boldsymbol{\beta}$	the $n \times 1$ vector containing $\beta^{e,f}$
$\boldsymbol{\Gamma}$	the *pseudo-inverse* of $\boldsymbol{\Lambda}$
η	non-dimensional variable of a plate in the y direction
$\theta_x(\xi,\eta)$	at location (ξ,η), rotational dof of a plate in the x direction
$\theta_y(\xi,\eta)$	at location (ξ,η), rotational dof of a plate in the y direction
$\theta_{xi}^{e,f}$	at the ith node, the rotational dof of the (e,f)th element in the x direction
$\theta_{yi}^{e,f}$	at the ith node, the rotational dof of the (e,f)th element in the y direction
$\kappa_x^{i,j}$	at the (i,j)th node, the curvature of a plate in the x direction
$\kappa_y^{i,j}$	at the (i,j)th node, the curvature of a plate in the y direction
$\boldsymbol{\kappa}^*$	the $m \times 1$ curvature vector of a damaged structure
$\boldsymbol{\Lambda}$	the $m \times n$ matrix denoting curvature of undamaged structure $(m>n)$
λ_i	the ith eigenvalue $(=\omega_i^2)$
v	the Poisson's ratio
ξ	non-dimensional variable of a plate in the x direction
σ_i	the ith singular value of $\boldsymbol{\Lambda}$
ρ	the density of a structure
$\boldsymbol{\upsilon}_i$	the $n \times 1$ vector denoting the ith basis of $\boldsymbol{\Lambda}^{\mathrm{T}}\boldsymbol{\Lambda}$
$\boldsymbol{\varphi}_i$	the ith mode shape vector
φ_{ji}	the jth component of the ith mode shape vector $(\boldsymbol{\varphi}_i)$
$\varphi_i(x,y)$	the function form of the ith mode shape
$\boldsymbol{\chi}(x,y)$	the 3×1 vector denoting curvature of a plate at location (x,y)
$\boldsymbol{\psi}_i$	the ith mass normalized mode shape vector
ψ_{ji}	the jth component of $\boldsymbol{\psi}_i$
ω_i	the ith natural frequency (rad/s)
$\boldsymbol{\Omega}$	the $r \times r$ diagonal matrix denoting singular values of $\boldsymbol{\Lambda}^{\mathrm{T}}\boldsymbol{\Lambda}$
a	the length of a rectangular plate element in the x direction
A	the cross-sectional area of a plate
b	the length of a rectangular plate element in the y direction
$\boldsymbol{B}(\xi,\eta)$	the 12×3 matrix denoting curvature of a plate at the location (ξ,η)
$\mathbf{C}$	the 12×12 matrix for a plate denoting linear relationship between $\boldsymbol{\alpha}$ and $\mathbf{w}^e$
D	a coefficient of material properties of a plate
$\boldsymbol{D}_1$	the 3×3 matrix denoting material properties of a plate
E	the Young's modulus
$\mathbf{e}$	the $m \times 1$ error vector
$\mathbf{E}$	mean squared error
$EI^{e,f}$	the flexural rigidity of the (e,f)th plate element
$\mathbf{F}$	the 8×8 element flexibility matrix of the rotational dof $(=\mathbf{S}^{-1})$
$\mathbf{G}$	the 8×4 matrix denoting the relationship between $\mathbf{w}_r^e$ and $\mathbf{w}_t^e$
h	the thickness of a plate
$\mathbf{H}$	the 8×12 plate element stiffness matrix of all the degrees of freedom
I	the sectional second moment of area
$\mathbf{K}$	the stiffness matrix
$\mathbf{K}^{-1}$	the flexibility matrix
m_i	the ith modal mass $(m_i = \boldsymbol{\varphi}_i^{\mathrm{T}}\mathbf{M}\boldsymbol{\varphi}_i)$
$\mathbf{M}$	the mass matrix
$\mathbf{M}(x,y)$	the 3×1 three internal moment vector per unit length at the location (x,y)
$\mathbf{M}_x^{i,j}$	at the $(i,\ j)$th node, the internal normal moments in the x direction
$\mathbf{M}_y^{i,j}$	at the (i,j)th node, the internal normal moments in the y direction
$\mathbf{N}(\xi,\eta)$	the 12×1 interpolation vector at the location (ξ,η)
$\mathbf{p}(\xi,\eta)$	the 12×1 polynomial state variable vector at the location (ξ,η)
$\mathbf{q}$	the $n \times 1$ vector denoting residual between $\boldsymbol{\beta}_0$ and $\boldsymbol{\beta}$

$\mathbf{R}$	a 8×8 diagonal matrix	$\mathbf{w}^e$	the 8×1 vector for a plate containing primary nodal variables
$\mathbf{S}$	the 8×8 element stiffness matrix of rotational dof	$w^{i,j}$	at the (i, j)th node in global coordinates, the transverse dof
$\mathbf{T}$	the 8×4 element stiffness matrix of transverse dof	$\mathbf{w}_r^e$	the 8×1 vector denoting the unmeasurable rotational dof
$\mathbf{Y}$	the $n \times r$ matrix denoting non-zero basis of $\mathbf{\Lambda}^{\mathrm{T}}\mathbf{\Lambda}$	$\mathbf{w}_t^e$	the 4×1 vector denoting the measurable transverse dof
$\mathbf{w}_k$	the kth modal flexibility vector		
$w(\xi, \eta)$	the transverse dof of a plate at the location (ξ, η)		

drawn special attention. The reason for this particular concern is traced to the results of the comparative full-scale damage detection study of Farrar and Jauregui [3]. The authors investigated the performance of five damage detection algorithms in blind mode using experimental data collected from a full-scale damage test. Based on the results, the authors concluded that the MSC method and the DI method are distinguishable. Such a memorable success of the MSC method and the DI method might be due to the sensitivity of curvature of mode shape with respect to the given damage. Since modal strain energy of the DI method is a function of curvature of mode shape, two methods basically utilize the measured curvature of mode shapes to evaluate damage.

Pandey et al. [1] suggested that the amount of damage in a structure could be obtained from the magnitude of changes in curvature of the mode shapes. In their numerical studies, the changes in resonant frequencies, Modal Assurance Criterion (MAC), Co-ordinate Modal Assurance (COMAC), displacement mode shapes did not indicate the presence of damage. Only changes in mode shape curvatures indicated damage. The MSC method utilizes the flexural formula for an Euler–Bernoulli beam and the curvature values are computed from the measured mode shape using the central difference approximation. Since the MSC method directly utilizes response data related to damage, no analytical model is required. This feature of the method renders the method potentially fast and cost-effective. In consequence, the MSC method has a great potential for on-line health monitoring of beam-like structures, since mode shapes can be extracted from the ambient vibration response of the structure. However, the MSC method has at least three shortcomings: first, the estimation results can be different if more than one mode is used [4]; second, in cases of a uniform reduction in the global stiffness, the method cannot predict such damage [5]; and third, the singularity problems near the inflection points of mode shapes are an obstacle to detecting damage [6]. For the mode selection problem, the work of Wahab and Roeck [7] proposes a curvature damage factor that is a linear summation of the difference in the curvature of mode shape for all modes. However, the proposed curvature damage factor has no physical interpretation.

Stubbs et al. [2] proposed the Damage Index (DI) method to locate and estimate damage using changes in the modal strain energy estimated from measured mode shapes. The method is based on an assumption of the invariance of the sensitivity of fractional modal strain energy of a potential damaged element during a small damage event. The feasibility and practicability of the DI method are demonstrated through a full-scale bridge by Stubbs et al. [8]. The theory is later

specialized for plates by Choi and Stubbs [9] and Cornwell et al. [10], frames by Stubbs et al. [11], trusses by Duffey et al. [12], and cylindrical shells by Srinivasan and Kot [13]. Apparently, the family of the DI method utilizing modal strain energy can be applied to any form of a structure in principle. Comparing to the MSC method, the DI method further requires the numerical integration of curvature of mode shape to obtain modal strain energy. This step might contribute to reduce the measurement noise. However, the singularity problem near inflection points and the mode selection problem still share with the MSC method.

The problem addressed in this study is to find changes in the stiffness of a structure given measured changes in the modal parameters. The objective of this study is to introduce a new technique that can detect, locate, and size damage for a selected class of structures. The proposed method basically shares with the same idea with the MSC method and the DI method, and possibly extends the efficiency, accuracy, and reliability of those methods by resolving the previously described deficiencies such as the mode selection problem and the singularity problem near inflection points of mode shape. One strategy taken in this study for the mode selection problem might exploit the concept of modal flexibility because modal flexibility is a rational way to combine the measured modes. In order to resolve the singularity problem, this study solves a governing equation of a damage mechanism that represents a rigorous structural relationship between changes in stiffness and changes in modal flexibility based on the fundamentals of structural mechanics.

To achieve the objective, the following five steps are performed. First, a few required assumptions and characteristics of modal flexibility are discussed. Second, the slope-deflection equation of a plate-like structure is derived from modal flexibility. Third, using the two-dimensional slop-deflection equation, a governing equation of damage mechanism, the so-called flexural damage index equation, is derived. Fourth, a special solution technique to the derived system of equation is presented. Finally, the numerical example is provided.

2. Theoritical background

2.1. Characteristics of modal flexibility

The global stiffness matrix ($\mathbf{K}$) and flexibility matrix ($\mathbf{K}^{-1}$) of a structure can be described in terms of natural frequencies and mode shapes [14] by

$$\mathbf{K} = \sum_{i=1}^{r} \frac{\omega_i^2}{m_i} \mathbf{M}\boldsymbol{\varphi}_i \boldsymbol{\varphi}_i^{\mathrm{T}} \mathbf{M} \tag{1}$$

and

$$\mathbf{K}^{-1} = \sum_{i=1}^{r} \frac{1}{m_i \omega_i^2} \boldsymbol{\varphi}_i \boldsymbol{\varphi}_i^{T}, \tag{2}$$

where the terms ω_i, $\boldsymbol{\varphi}_i$, and m_i are the ith natural frequency, mode shape vector, and modal mass, respectively. The scalar, r, denotes the number of mode considered. The matrix $\mathbf{M}$ denotes the

global mass matrix of a structure. It can be seen that the dynamically measured flexibility matrix has at least the following five features:

First, *dominance of the low frequency*: the ith modal contribution factor, $1/(m_i\omega_i^2)$, of the flexibility matrix rapidly decreases as the frequency increases. However, the ith contribution factor, ω_i^2/m_i, of the stiffness matrix increases as frequency increases. Thus, the flexibility matrix can be accurately synthesized from a few of the lower frequencies and mode shapes even if the stiffness matrix can be accurately synthesized from high frequency modes.

Second, *uncoupling with the mass matrix*: the ith modal contribution matrix, $\boldsymbol{\varphi}_i\boldsymbol{\varphi}_i^{\mathrm{T}}$, of the flexibility matrix is not coupled with the mass matrix unlike the modal contribution matrix, $\mathbf{M}\boldsymbol{\varphi}_i\boldsymbol{\varphi}_i^{\mathrm{T}}\mathbf{M}$, of the stiffness matrix. Thus, the flexibility matrix is less sensitive to a local change of mass although its overall magnitude is scaled by the ith modal contribution factor, $1/(m_i\omega_i^2)$.

Third, *independence of the probing degree of freedom*: one of the more important features is a relaxation of the number of degree of freedom (dof) required to measure the modal flexibility. Since the flexibility matrix is an inverse of the stiffness matrix, each component of the flexibility matrix is a fractional number. Its denominator is a characteristic equation that is a function of the local structural rigidities. Thus, any local stiffness is detectable in any dof if the flexibility matrix is directly used. However, the local stiffness in the global stiffness matrix is located in a diagonal band without the characteristic equation in the case of a straight beam. Hence, the ith local stiffness cannot be detected in the jth dof if the jth dof is not a neighbor of the ith dof.

Fourth, *linearity*: the dynamically measured modal flexibility can be linearly decomposed into bending flexibility, torsional flexibility, and axial flexibility corresponding to its bases. Thus, the damage and boundary condition can be independently dealt with its characteristic mode. In addition, the reciprocal theorem is still valid because of the symmetry.

Finally, *transformation from dynamic domain to static domain*: the modal flexibility can be interpreted as a domain transformation from the dynamic domain to the static domain, since dynamically measured modal flexibility represents a static deflection profile caused by a unit load. This property is important in vibration-based nondestructive damage evaluation because a single representative solution can be obtained by combining the results estimated from each mode.

The kth column of the flexibility matrix in Eq. (2) can be interpreted as a displacement vector due to a unit load at the kth dof. The modal approximation of the kth column of the flexibility matrix can be called the kth modal flexibility vector here. Note that the kth modal flexibility vector can also be represented by a matrix form with respect to two-dimensional coordinates (x and y). Hence, in the followings, the kth modal flexibility vector will be equivalently called the (i, j)th modal flexibility matrix that is a displacement matrix caused by a unit load at (i, j)th node.

Then the kth modal flexibility vector, denoted by $\mathbf{w}_k$, can be obtained from Eq. (2) as follows:

$$\mathbf{w}_k = \sum_{i=1}^{r} \frac{\varphi_{ki}}{\lambda_i m_i}\boldsymbol{\varphi}_i, \tag{3}$$

where the scalar, φ_{ki}, is the kth component of the ith mode shape, and $\lambda_i(=\omega_i^2)$ denotes the eigenvalue of the ith mode.

Since the relationship between the mass normalized mode shape for the ith mode, $\boldsymbol{\psi}_i$, and its general form, $\boldsymbol{\varphi}_i$, is $\boldsymbol{\varphi}_i = \sqrt{m_i}\boldsymbol{\psi}_i$ [15], the kth modal flexibility vector can also be expressed in terms of mass normalized mode shapes:

$$\mathbf{w}_k = \sum_{i=1}^{r} \frac{\psi_{ki}}{\lambda_i} \boldsymbol{\psi}_i. \tag{4}$$

2.2. Modal mass approximation

If both input and output measurements are available, many modal analysis packages provide the mass normalized mode shapes without absolute value of modal mass, because the identified modal mass has no physical meaning except for scaling mode shapes. In a forced vibration test, the kth modal flexibility vector can be obtained by Eq. (4) instead of the generalized form of Eq. (3). If mode shapes and natural frequencies are estimated from output-only ambient response, there is no way to find the modal mass because the residue of the transfer function cannot be estimated. However, if we assume that the mass density of a structure has not changed during a small damage event, the ith modal mass for a uniform thin plate can be obtained accurately by a numerical integration of the following formula:

$$m_i = \int_A \rho h \varphi_i \varphi_i \, \mathrm{d}A, \tag{5}$$

where the terms, ρ, h, and A denote, respectively, the density, the thickness, and the area of the plate. The function $\varphi_i(x, y)$ denotes the ith mode shape. To approximate the ith modal mass, a double integration is required. One of the easiest ways is to use the trapezoidal rule twice. First, the discrete measurements of the ith mode shape can be interpolated with respect to the y direction using the *cubic Spline* function. This step is necessary because the sensor spacing is typically coarse in practice. Second, the interpolated mode shapes can be integrated with respect to the y direction using the trapezoidal integration rule after squaring the interpolated mode shapes. Next, the same procedures are repeated in the x direction. Third, the *cubic Spline* interpolation with respect to the x direction for the resulting integrated values is performed. Finally, the trapezoidal integration with respect to the x direction yields the ith approximate modal mass.

2.3. Small damage assumption

The small deflection theory assumes that the change in shape of a structure due to a force must not affect the line of action of the applied loads [16]. Hence, the internal forces of a deformable body caused by the applied loads can be obtained from initial configuration. As an extension of such an assumption, one may assume that the additional change in shape of a structure due to a small damage event under a given loading condition may also not affect the line of the action of the applied loads. In other words, the effect of the additional change in shape on the line of the action of the applied loads may be considered to be secondary. Based on such a consideration, two assumptions will be made here. First, a small damage event, a priori, will have an insignificant effect on the internal forces of a statically determinate linear structure. Second, it is also assumed that the same is true in a statically indeterminate linear structure.

2.4. Two-dimensional slope-deflection equation

Two-dimensional plate modes are often encountered for a structure in which length and width are large compared to the thickness (e.g. the plate-like bridge). The objective of this section is to derive the slope-deflection equation for a plate-like structure. Consider the isotropic thin plate shown in Fig. 1. Assume that the static deflection profile, denoted by $w(x, y)$, due to a unit load at the (i, j)th node, is accurately approximated at the discrete measurement position utilizing the kth modal flexibility vector, $\mathbf{w}_k$, (i.e. the (i,j)th modal flexibility matrix) in Eq. (3) or Eq. (4).

The transverse deflection, $w(x, y)$, of the plate element 'A' is governed by the fourth-order differential equation:

$$D\nabla^4 w = f_z, \tag{6}$$

where

$$D = \frac{Eh^3}{12(1-v^2)} \text{ and } \nabla^4 = \frac{\partial^4}{\partial x^4} + 2\frac{\partial^4}{\partial x^2 \partial y^2} + \frac{\partial^4}{\partial y^4}.$$

The applied force, f_z, will be zero except at the (i,j)th node. The terms, E, v, and h denote Young's modulus, the Poisson's ratio, and thickness of the plate, respectively. The constitutive laws related to internal moments ($\mathbf{M}_x$, $\mathbf{M}_y$, and $\mathbf{M}_{xy}$), with a sign convention shown in Fig. 2, and the respective curvatures are as follows:

$$\mathbf{M}(x, y) = \boldsymbol{D}_1 \boldsymbol{\chi}(x, y), \tag{7}$$

where

$$\boldsymbol{D}_1 = D\begin{bmatrix} 1 & v & 0 \\ v & 1 & 0 \\ 0 & 0 & \dfrac{(1-v)}{2} \end{bmatrix}, \tag{8}$$

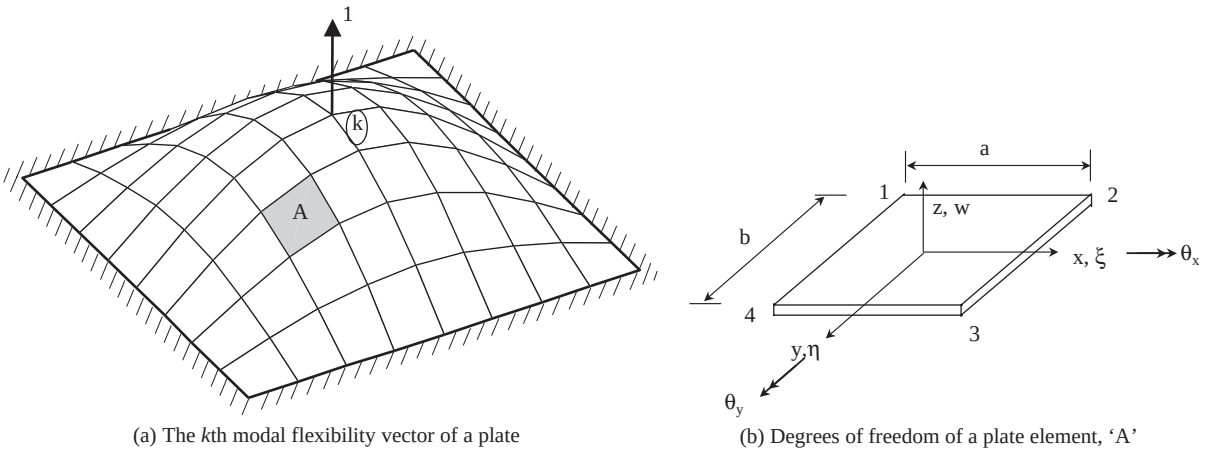

(a) The kth modal flexibility vector of a plate

(b) Degrees of freedom of a plate element, 'A'

Fig. 1. The kth modal flexibility vector of an engineering plate.

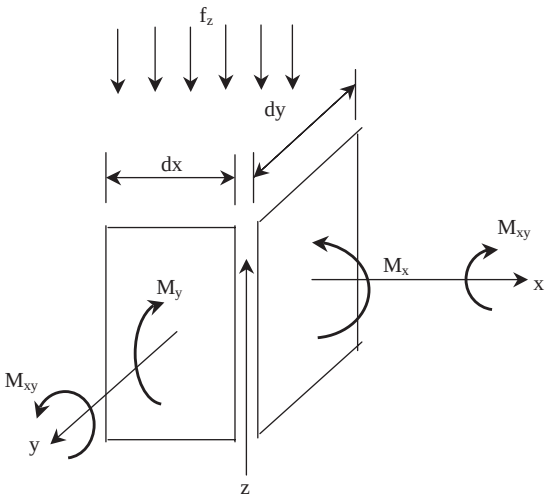

Fig. 2. Sign convention of a differential element.

$$\chi(x,y) = \left[-\frac{\partial^2 w}{\partial x^2} \quad -\frac{\partial^2 w}{\partial y^2} \quad -2\frac{\partial^2 w}{\partial x \partial y} \right]^{\mathrm{T}}. \tag{9}$$

The 3×1 vector, $\mathbf{M}(x,y) = [\mathbf{M}_x \quad \mathbf{M}_y \quad \mathbf{M}_{xy}]^{\mathrm{T}}$, denotes the internal moments per unit length. The 3×3 matrix, $\boldsymbol{D}_1$, denotes the material properties for the plate and the 3×1 vector, $\boldsymbol{\chi}(x,y)$, denotes the curvature of the plate. For numerical convenience, the non-dimensional local coordinate system shown in Fig. 1b will be used in the following discussion. There are three degrees of freedom at each node. The transverse deflection normal to the middle surface of the plate, $w(x,y)$, and the two rotational dof $\theta_x = \partial w/\partial y$ and $\theta_y = -\partial w/\partial x$. The non-dimensional variables in Fig. 1b are defined as

$$\xi = \frac{2}{a}x, \quad \eta = \frac{2}{b}y, \tag{10}$$

where the 'a' and 'b' denote the length of the plate element with respect to x and y direction, respectively. It can be seen that the primary nodal variables of the plate element are as follows

$$w(\xi,\eta), \quad \theta_x(\xi,\eta) = \frac{2}{b}\frac{\partial w}{\partial \eta}, \quad \theta_y(\xi,\eta) = -\frac{2}{a}\frac{\partial w}{\partial \xi}. \tag{11}$$

Thus, we have 12 nodal dof for one plate element:

$$w(-1,-1) \equiv w_1, \quad \theta_x(-1,-1) \equiv \theta_{x1}, \quad \theta_y(-1,-1) \equiv \theta_{y1}, \tag{12}$$

$$w(1,-1) \equiv w_2, \quad \theta_x(1,-1) \equiv \theta_{x2}, \quad \theta_y(1,-1) \equiv \theta_{y2}, \tag{13}$$

$$w(1,1) \equiv w_3, \quad \theta_x(1,1) \equiv \theta_{x3}, \quad \theta_y(1,1) \equiv \theta_{y3}, \tag{14}$$

$$w(-1,1) \equiv w_4, \quad \theta_x(-1,1) \equiv \theta_{x4}, \quad \theta_y(-1,1) \equiv \theta_{y4}. \tag{15}$$

Since the element has a total of 12 dof, the transverse deflection, $w(\xi,\eta)$, can be represented by a polynomial having 12 terms. In addition, the complete polynomial with cubic dof should be considered for homogeneous solution of the fourth-order partial differential equation. Here, the complete polynomials in two variables can be generated by Pascal's triangle. However, the complete cubic polynomial has only 10 polynomial terms. Thus, two more terms should be added to the complete cubic polynomial. The potential candidates for such an addition are $\xi^3\eta$, $\xi^2\eta^2$, and $\xi\eta^3$. However, the choice of the term, $\xi^2\eta^2$, should be excluded because the term, $\xi^2\eta^2$, does not satisfy the homogeneous partial differential equation (especially the second term, $\partial^4/\partial\xi^2\partial\eta^2$, in ∇^4 is not zero but unity) and there is no reason to choose the unsymmetric polynomial. Therefore, the homogeneous solution can be expressed by adding the symmetric two terms $\{\xi^3\eta, \xi\eta^3\}$ to the complete cubic polynomial:

$$w(\xi,\eta) \equiv \mathbf{p}(\xi,\eta)^{\mathrm{T}}\boldsymbol{\alpha}, \tag{16}$$

where the 12×1 vector, $\boldsymbol{\alpha} = [\alpha_1,\alpha_2,\alpha_3,\alpha_4,\alpha_5,\alpha_6,\alpha_7,\alpha_8,\alpha_9,\alpha_{10},\alpha_{11},\alpha_{12}]^{\mathrm{T}}$, denotes the unknown coefficients. The 12×1 vector, $\mathbf{p} = [1,\xi,\eta,\xi^2,\xi\eta,\eta^2,\xi^3,\xi^2\eta,\xi\eta^2,\eta^3,\xi^3\eta,\xi\eta^3]^{\mathrm{T}}$, denotes the polynomial state variable. The next step involves expressing $\boldsymbol{\alpha}$ in terms of the primary nodal variables $(w_1,\theta_{x1},\theta_{y1},w_2,\theta_{x2},\theta_{y2},w_3,\theta_{x3},\theta_{y3},w_4,\theta_{x4},\theta_{y4})$. Substituting Eq. (16) into the boundary conditions from Eq. (12) into Eq. (15) yields

$$\mathbf{R}\mathbf{w}^e = \mathbf{C}\boldsymbol{\alpha}, \tag{17}$$

where the 12×12 matrix, $\mathbf{R}$, is a diagonal matrix whose components are $\mathbf{R} = \mathrm{diag}[1, b/2, a/2, 1, b/2, a/2, 1, b/2, a/2, 1, b/2, a/2]$. The 12×1 vector, $\mathbf{w}^e = [w_1,\theta_{x1},\theta_{y1},w_2,\theta_{x2},\theta_{y2},w_3,\theta_{x3},\theta_{y3},w_4,\theta_{x4},\theta_{y4}]^{\mathrm{T}}$, denotes the primary nodal variables at the nodes. Thus, the coefficient vector, $\boldsymbol{\alpha}$, can be directly obtained by inverting the constant matrix, $\mathbf{C}$.

$$\boldsymbol{\alpha} = \mathbf{C}^{-1}\mathbf{R}\mathbf{w}^e. \tag{18}$$

Substitution of Eq. (18) into Eq. (16) yields the transverse deflection, $w(\xi,\eta)$, in terms of the primary nodal variables.

$$w(\xi,\eta) = \mathbf{N}(\xi,\eta)^{\mathrm{T}}\mathbf{w}^e, \tag{19}$$

where the 12×1 matrix, $\mathbf{N}(\xi,\eta) = \mathbf{R}\mathbf{C}^{-\mathrm{T}}\mathbf{p}(\xi,\eta)$ is an interpolation matrix. Now, we can estimate the transverse deflection at any point inside the plate element if we can measure all the dof. The next step involves expressing the resultant stresses in terms of the primary nodal variables by applying the constitutive law. Substituting Eq. (19) into the curvature vector into Eq. (9) yields

$$\boldsymbol{\chi}(\xi,\eta) = \mathbf{B}(\xi,\eta)^{\mathrm{T}}\mathbf{w}^e, \tag{20}$$

where the 12×3 matrix, $\mathbf{B}(\xi,\eta) = \left[-\frac{4}{a^2}\frac{\partial^2\mathbf{N}}{\partial\xi^2} \quad -\frac{4}{b^2}\frac{\partial^2\mathbf{N}}{\partial\eta^2} \quad -\frac{4}{ab}2\frac{\partial^2\mathbf{N}}{\partial\xi\,\partial\eta}\right]$, denotes the curvature of the interpolation functions. The substitution of the curvature vector in Eq. (20), into the constitutive law in Eq. (7) yields

$$\mathbf{M}(\xi,\eta) = \boldsymbol{D}_1\mathbf{B}(\xi,\eta)^{\mathrm{T}}\mathbf{w}^e. \tag{21}$$

This equation represents the relationship between the resultant stresses (internal moment per unit length) and the primary nodal variables. Thus, we are ready to estimate the internal moment at any point inside the plate element if we measure all the dof at the four nodes. Using Eq. (21),

the internal moments at the four nodes can be evaluated at $\xi = \pm 1, \eta = \pm 1$.

$$\mathbf{M}_1 = \boldsymbol{D}_1 \mathbf{B}(-1,-1)^{\mathrm{T}} \mathbf{w}^e, \tag{22}$$

$$\mathbf{M}_2 = \boldsymbol{D}_1 \mathbf{B}(1,-1)^{\mathrm{T}} \mathbf{w}^e, \tag{23}$$

$$\mathbf{M}_3 = \boldsymbol{D}_1 \mathbf{B}(1,1)^{\mathrm{T}} \mathbf{w}^e, \tag{24}$$

$$\mathbf{M}_4 = \boldsymbol{D}_1 \mathbf{B}(-1,1)^{\mathrm{T}} \mathbf{w}^e, \tag{25}$$

where the 3×1 matrices, $\mathbf{M}_i = [\mathbf{M}_{xi}, \mathbf{M}_{yi}, \mathbf{M}_{xyi}]^{\mathrm{T}}$, denotes the internal moments at the ith node. Here, denoting the local node of the plate, the subscript, i, is used as an iteration index varying from 1 to 4. For example, $\mathbf{M}_{x2}$ $(i = 2)$ denotes the resulting normal moment at the node 2 in the x direction of local coordinate system. The next step involves expressing the rotational degrees of freedom in terms of the internal moments and the measurable degrees of freedom. Since $\mathbf{M}_{xy} = -\mathbf{M}_{yx}$, the twisting moment at each node yields identical equations. Therefore, a singularity problem arises if one inverts the element stiffness matrix of all the degrees of freedom. The reason for this problem may be traced to the fact that the considered plate element is non-conforming. Ignoring the constraint information from twisting moments, $\mathbf{M}_{xyi}$, we only consider the normal moments, $\mathbf{M}_{xi}$ and $\mathbf{M}_{yi}$ at the four nodes. The reason for this treatment is traced to the fact that the contribution of the twisting moments, $\mathbf{M}_{xyi}$, on the deformation profile of a thin plate is insignificant compared to the normal moments, $\mathbf{M}_{xi}$ and $\mathbf{M}_{yi}$. Taking only the normal moments, $\mathbf{M}_{xi}$ and $\mathbf{M}_{yi}$, from Eq. (22) to Eq. (25) yields

$$\mathbf{M}^e = \mathbf{H}\mathbf{w}^e, \tag{26}$$

where the 8×1 vector, $\mathbf{M}^e = [\mathbf{M}_{x1}, \mathbf{M}_{y1}, \mathbf{M}_{x2}, \mathbf{M}_{y2}, \mathbf{M}_{x3}, \mathbf{M}_{y3}, \mathbf{M}_{x4}, \mathbf{M}_{y4}]^{\mathrm{T}}$, denotes the normal stress resultants at the four nodes. The 8×12 matrix, $\mathbf{H}$, denotes the element stiffness matrix of all the degrees of freedom, and can be decomposed with respect to the measurable and un-measurable dof.

$$\mathbf{M}^e = \mathbf{S}\mathbf{w}_r^e + \mathbf{T}\mathbf{w}_t^e, \tag{27}$$

where the 4×1 vector, $\mathbf{w}_t^e = [w_1, w_2, w_3, w_4]^{\mathrm{T}}$, denotes the measurable transverse dof. The 8×1 matrix, $\mathbf{w}_r^e = [\theta_{x1}, \theta_{y1}, \theta_{x2}, \theta_{y2}, \theta_{x3}, \theta_{y3}, \theta_{x4}, \theta_{y4}]^{\mathrm{T}}$, denotes the un-measurable rotational dof. The 8×8 matrix, $\mathbf{S}$, denotes the partitioned element stiffness matrix of the rotational dof. The 8×4 matrix, $\mathbf{T}$, denotes the partitioned stiffness matrix of the transverse dof. The rotational dof can be expressed by

$$\mathbf{w}_r^e = \mathbf{F}\mathbf{M}^e + \mathbf{G}\mathbf{w}_t^e \tag{28}$$

where the 8×8 matrix, $\mathbf{F} = \mathbf{S}^{-1}$, denotes the element flexibility matrix of the rotational dof. The 8×4 matrix, $\mathbf{G} = -\mathbf{F}\mathbf{T}$, denotes the relationship between the rotational dof and the transverse dof. For simplicity, we may define a sectional second moment of area per unit length as

$I = 1 \times h^3/12$. The explicit expression of Eq. (28) is as follows:

$$\begin{bmatrix} \theta_{x1} \\ \theta_{y1} \\ \theta_{x2} \\ \theta_{y2} \\ \theta_{x3} \\ \theta_{y3} \\ \theta_{x4} \\ \theta_{y4} \end{bmatrix} = \begin{bmatrix} -\frac{vb}{3EI} & \frac{b}{3EI} & 0 & 0 & 0 & 0 & -\frac{vb}{6EI} & \frac{b}{6EI} \\ -\frac{a}{3EI} & \frac{va}{3EI} & -\frac{a}{6EI} & \frac{va}{6EI} & 0 & 0 & 0 & 0 \\ 0 & 0 & -\frac{vb}{3EI} & \frac{b}{3EI} & -\frac{vb}{6EI} & \frac{b}{6EI} & 0 & 0 \\ \frac{a}{6EI} & -\frac{va}{6EI} & \frac{a}{3EI} & -\frac{va}{3EI} & 0 & 0 & 0 & 0 \\ 0 & 0 & \frac{vb}{6EI} & -\frac{b}{6EI} & \frac{vb}{3EI} & -\frac{b}{3EI} & 0 & 0 \\ 0 & 0 & 0 & 0 & \frac{a}{3EI} & -\frac{va}{3EI} & \frac{a}{6EI} & -\frac{va}{6EI} \\ \frac{vb}{6EI} & -\frac{b}{6EI} & 0 & 0 & 0 & 0 & \frac{vb}{3EI} & -\frac{b}{3EI} \\ 0 & 0 & 0 & 0 & -\frac{a}{6EI} & \frac{va}{6EI} & -\frac{a}{3EI} & \frac{va}{3EI} \end{bmatrix} \begin{bmatrix} \mathbf{M}_{x1} \\ \mathbf{M}_{y1} \\ \mathbf{M}_{x2} \\ \mathbf{M}_{y2} \\ \mathbf{M}_{x3} \\ \mathbf{M}_{y3} \\ \mathbf{M}_{x4} \\ \mathbf{M}_{y4} \end{bmatrix} + \begin{bmatrix} -\frac{1}{b} & 0 & 0 & \frac{1}{b} \\ \frac{1}{a} & -\frac{1}{a} & 0 & 0 \\ 0 & -\frac{1}{b} & \frac{1}{b} & 0 \\ \frac{1}{a} & -\frac{1}{a} & 0 & 0 \\ 0 & -\frac{1}{b} & \frac{1}{b} & 0 \\ 0 & 0 & -\frac{1}{a} & \frac{1}{a} \\ -\frac{1}{b} & 0 & 0 & \frac{1}{b} \\ 0 & 0 & -\frac{1}{a} & \frac{1}{a} \end{bmatrix} \begin{bmatrix} w_1 \\ w_2 \\ w_3 \\ w_4 \end{bmatrix}. \tag{29}$$

This equation will be referred to here as the two-dimensional slope-deflection equation for a thin plate.

2.5. Flexural damage index equation

The objective of this section is to derive a set of damage index equations from previously derived slope-deflection equation (29). Consider the four rectangular elements shown in Fig. 3. A transformation from local coordinates to global coordinates is shown in Table 1. For the (e, $f+1$)th element, the first row in Eq. (29) in global coordinates becomes

$$\theta_{x1}^{e,f+1} = -\frac{vb\mathbf{M}_x^{i-1,j}}{3EI^{e,f+1}} + \frac{b\mathbf{M}_y^{i-1,j}}{3EI^{e,f+1}} - \frac{vb\mathbf{M}_x^{i-1,j+1}}{6EI^{e,f+1}} + \frac{b\mathbf{M}_y^{i-1,j+1}}{6EI^{e,f+1}} + \frac{w^{i-1,j+1} - w^{i-1,j}}{b}. \tag{30}$$

Similarly, for the (e, f)th element, the seventh row of Eq. (29) in a global coordinate becomes

$$\theta_{x4}^{e,f} = \frac{vb\mathbf{M}_x^{i-1,j}}{3EI^{e,f}} - \frac{b\mathbf{M}_y^{i-1,j}}{3EI^{e,f}} + \frac{vb\mathbf{M}_x^{i-1,j-1}}{6EI^{e,f}} - \frac{b\mathbf{M}_y^{i-1,j-1}}{6EI^{e,f}} + \frac{w^{i-1,j} - w^{i-1,j-1}}{b}. \tag{31}$$

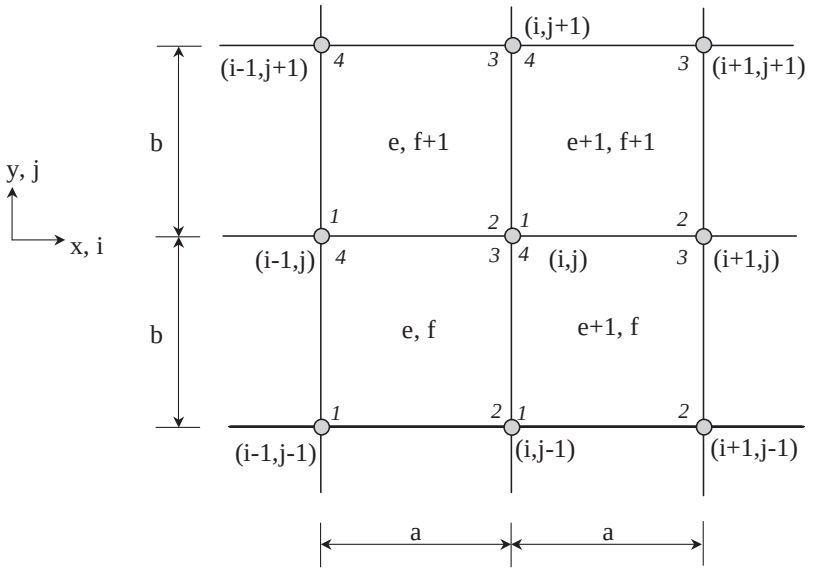

Fig. 3. Global coordinates of the plate elements.

Table 1
Coordinate transformation of a plate

	Elements			
	(e,f)	$(e+1,f)$	$(e,f+1)$	$(e+1,f+1)$
$\mathbf{M}_{x1}$	$\mathbf{M}_x^{i-1,j-1}$	$\mathbf{M}_x^{i,j-1}$	$\mathbf{M}_x^{i-1,j}$	$\mathbf{M}_x^{i,j}$
$\mathbf{M}_{y1}$	$\mathbf{M}_y^{i-1,j-1}$	$\mathbf{M}_y^{i,j-1}$	$\mathbf{M}_y^{i-1,j}$	$\mathbf{M}_y^{i,j}$
$\mathbf{M}_{x2}$	$\mathbf{M}_x^{i,j-1}$	$\mathbf{M}_x^{i+1,j-1}$	$\mathbf{M}_x^{i,j}$	$\mathbf{M}_x^{i+1,j}$
$\mathbf{M}_{y2}$	$\mathbf{M}_y^{i,j-1}$	$\mathbf{M}_y^{i+1,j-1}$	$\mathbf{M}_y^{i,j}$	$\mathbf{M}_y^{i+1,j}$
$\mathbf{M}_{x3}$	$\mathbf{M}_x^{i,j}$	$\mathbf{M}_x^{i+1,j}$	$\mathbf{M}_x^{i,j+1}$	$\mathbf{M}_x^{i+1,j+1}$
$\mathbf{M}_{y3}$	$\mathbf{M}_y^{i,j}$	$\mathbf{M}_y^{i+1,j}$	$\mathbf{M}_y^{i,j+1}$	$\mathbf{M}_y^{i+1,j+1}$
$\mathbf{M}_{x4}$	$\mathbf{M}_x^{i-1,j}$	$\mathbf{M}_x^{i,j}$	$\mathbf{M}_x^{i-1,j+1}$	$\mathbf{M}_x^{i,j+1}$
$\mathbf{M}_{y4}$	$\mathbf{M}_y^{i-1,j}$	$\mathbf{M}_y^{i,j}$	$\mathbf{M}_y^{i-1,j+1}$	$\mathbf{M}_y^{i,j+1}$
w_1	$w^{i-1,j-1}$	$w^{i,j-1}$	$w^{i-1,j}$	$w^{i,j}$
w_2	$w^{i,j-1}$	$w^{i+1,j-1}$	$w^{i,j}$	$w^{i+1,j}$
w_3	$w^{i,j}$	$w^{i+1,j}$	$w^{i,j+1}$	$w^{i+1,j+1}$
w_4	$w^{i-1,j}$	$w^{i,j}$	$w^{i-1,j+1}$	$w^{i,j+1}$

Since the slopes for elements $(e,f+1)$ and (e,f) are the same at the $(i\text{-}1,j)$th node in the y direction, we have the continuity condition:

$$\theta_{x1}^{e,f+1} = \theta_{x4}^{e,f}. \tag{32}$$

After substituting Eqs. (30) and (31) into Eq. (32), the rearrangement with respect to the flexural rigidity of each element yields the following equation for a damaged structure:

$$\left(v\bar{\mathbf{M}}_x^{i-1,j-1}+2v\bar{\mathbf{M}}_x^{i-1,j}-\bar{\mathbf{M}}_y^{i-1,j-1}-2\bar{\mathbf{M}}_y^{i-1,j}\right)\frac{1}{\overline{EI}^{e,f}}+\left(2v\bar{\mathbf{M}}_x^{i-1,j}+v\bar{\mathbf{M}}_x^{i-1,j+1}-2\bar{\mathbf{M}}_y^{i-1,j}-\bar{\mathbf{M}}_y^{i-1,j+1}\right)\frac{1}{\overline{EI}^{e,f+1}}$$
$$=6\frac{\bar{w}^{i-1,j-1}-2\bar{w}^{i-1,j}+\bar{w}^{i-1,j+1}}{b^2}, \tag{33}$$

where the upper bar denotes damage. Using the application of the small damage assumption, $\mathbf{M}\approx\bar{\mathbf{M}}$, yields

$$\left(v\mathbf{M}_x^{i-1,j-1}+2v\mathbf{M}_x^{i-1,j}-\mathbf{M}_y^{i-1,j-1}-2\mathbf{M}_y^{i-1,j}\right)\frac{1}{\overline{EI}^{e,f}}+\left(2v\mathbf{M}_x^{i-1,j}+v\mathbf{M}_x^{i-1,j+1}-2\mathbf{M}_y^{i-1,j}-\mathbf{M}_y^{i-1,j+1}\right)\frac{1}{\overline{EI}^{e,f+1}}$$
$$=6\frac{\bar{w}^{i-1,j-1}-2\bar{w}^{i-1,j}+\bar{w}^{i-1,j+1}}{b^2}. \tag{34}$$

Note that the right-hand side of Eq. (34) (ignoring the constant (6)) is a central difference approximation of the curvature of the damaged structure at the $(i-1,j)$th node. The well known moment–curvature relationship at the $(i-1, j)$th node is given by

$$\mathbf{M}_x^{i-1,j-1}=-\frac{EI^{e,f}}{(1-v^2)}(\kappa_x^{i-1,j-1}+v\kappa_y^{i-1,j-1}), \tag{35}$$

$$\mathbf{M}_x^{i-1,j}=-\frac{EI^{e,f}}{(1-v^2)}(\kappa_x^{i-1,j}+v\kappa_y^{i-1,j}), \tag{36}$$

$$\mathbf{M}_y^{i-1,j-1}=-\frac{EI^{e,f}}{(1-v^2)}(\kappa_y^{i-1,j-1}+v\kappa_x^{i-1,j-1}), \tag{37}$$

$$\mathbf{M}_y^{i-1,j}=-\frac{EI^{e,f}}{(1-v^2)}(\kappa_y^{i-1,j}+v\kappa_x^{i-1,j}), \tag{38}$$

$$\mathbf{M}_x^{i-1,j}=-\frac{EI^{e,f+1}}{(1-v^2)}(\kappa_x^{i-1,j}+v\kappa_y^{i-1,j}), \tag{39}$$

$$\mathbf{M}_x^{i-1,j+1}=-\frac{EI^{e,f+1}}{(1-v^2)}(\kappa_x^{i-1,j+1}+v\kappa_y^{i-1,j+1}), \tag{40}$$

$$\mathbf{M}_y^{i-1,j}=-\frac{EI^{e,f+1}}{(1-v^2)}(\kappa_y^{i-1,j}+v\kappa_x^{i-1,j}), \tag{41}$$

$$\mathbf{M}_y^{i-1,j+1}=-\frac{EI^{e,f+1}}{(1-v^2)}(\kappa_y^{i-1,j+1}+v\kappa_x^{i-1,j+1}). \tag{42}$$

If $\bar{\kappa}_y^{i-1,j}$ denotes the curvature of damaged structure at the $(i-1, j)$th node, the substitution of the moment–curvature relationships from Eq. (35) to Eq. (42) into Eq. (34) yields the

two-dimensional Flexural Damage Index Equation (FDIE) in the y direction at the $i-1$ lane:

$$(\kappa_y^{i-1,j-1} + 2\kappa_y^{i-1,j})\beta^{e,f} + (2\kappa_y^{i-1,j} + \kappa_y^{i-1,j+1})\beta^{e,f+1} = 6\bar{\kappa}_y^{i-1,j}, \tag{43}$$

where

$$\beta^{e,f} = EI^{e,f}/\overline{EI}^{e,f} \tag{44}$$

denotes a flexural damage index of the (e, f)th element. Since the slopes for elements $(e, f+1)$ and (e, f) are the same at the (i, j)th node in the y direction, we have the continuity condition:

$$\theta_{x2}^{e,f+1} = \theta_{x3}^{e,f}. \tag{45}$$

The same manipulation from Eq. (30) to Eq. (42) yields the two-dimensional FDIE in the y direction at the ith lane:

$$(\kappa_y^{i,j-1} + 2\kappa_y^{i,j})\beta^{e,f} + (2\kappa_y^{i,j} + \kappa_y^{i,j+1})\beta^{e,f+1} = 6\bar{\kappa}_y^{i,j}. \tag{46}$$

Similarly, the slopes, θ_y, at the (i, j)th node to the $(i, j-1)$th node should be continuous. For the plate problem, two continuity conditions are available in x direction. One continuity condition at the (i, j)th node in the x direction is $\theta_{y3}^{e,f} = \theta_{y4}^{e+1,f}$, which results in

$$(\kappa_x^{i-1,j} + 2\kappa_x^{i,j})\beta^{e,f} + (2\kappa_x^{i,j} + \kappa_x^{i+1,j})\beta^{e+1,f} = 6\bar{\kappa}_x^{i,j}. \tag{47}$$

The other continuity condition at the $(i, j-1)$th node in the x direction is $\theta_{y2}^{e,f} = \theta_{y1}^{e+1,f}$, which yields

$$(\kappa_x^{i-1,j-1} + 2\kappa_x^{i,j-1})\beta^{e,f} + (2\kappa_x^{i,j-1} + \kappa_x^{i+1,j-1})\beta^{e+1,f} = 6\bar{\kappa}_x^{i,j-1}. \tag{48}$$

From the derived FDIE of the plate, the following observations can be made:

1. the damage index equations in the two directions are uncoupled
2. the damage indices of two lanes in each direction are correlated
3. the Poisson's ratio does not appear in the resulting equations.

For each direction, two coupled FDIEs are available. The deflection profile of those lanes can be partitioned from the (i,j)th modal flexibility matrix (i.e. kth modal flexibility vector). It is noted that accuracy depends on measurement spacing, since the central approximation is applied in both sides of the damage index equation. To achieve a good curvature profile from coarse measurement spacing, *cubic Spline* interpolation of the (i,j)th modal flexibility matrix is a prerequisite before applying the central difference formula to obtain curvature profile. In addition, the assumed density of a structure used for scaling the modal flexibility will cancel out in the two sides of the FDIEs, because the density of structure is assumed to be a constant for small damage events. Hence, the identified damage indices do not depend on the modal mass uncertainty, although the modal flexibility is affected by the uncertainty about modal mass for output-only modal analysis.

Suppose that the interpolated number of measurement locations are N_x and N_y in the x and y direction, respectively. For the (i,j)th modal flexibility matrix, the number of the coupled FDIE is $2 \times (N_x - 2)$ for one node lane in the x direction because the equations at two boundary nodes are not applicable $(N_x - 2)$ and two equations are available for one node lane. Since there are N_y lanes in the y direction, the possible number of the equation is $2 \times (N_x - 2) \times (N_y - 2)$ for the x direction of the (i,j)th modal flexibility matrix. Therefore, the total possible number of the

equation becomes $4 \times (N_x - 2)^2 \times (N_y - 2)^2$ for the (i,j)th modal flexibility matrix because the same number of equations are available in the y direction. Furthermore, the set of damage index equations is also valid for the $(i+1, j+1)$th modal flexibility matrix. If the available number of modal flexibility matrix is N_f, the available number of FDIE is $4 \times (N_x - 2)^2 \times (N_y - 2)^2 \times N_f$ denoted by m. However, the number of unknown damage indices, $\boldsymbol{\beta}$, is only $(N_x - 1) \times (N_y - 1)$ denoted by n. Therefore, the sufficient number of interpolated equations is available. Thus, a set of coupled FDIEs at each interpolated location results in an over-determined system of linear equations:

$$\boldsymbol{\Lambda\beta} = \boldsymbol{\kappa}^*, \tag{49}$$

where the $n \times 1$ vector, $\boldsymbol{\beta}$, denotes the damage index vector to be evaluated, and $m \times 1$ vector, $\boldsymbol{\kappa}^*$, denotes a curvature vector of the damaged structure. The $m \times n$ matrix, $\boldsymbol{\Lambda}$, represents a curvature set for the undamaged structure.

The maximum rank of the matrix $\boldsymbol{\Lambda}$ is only n. In principle, the solutions for a set of linear algebraic equations are identical if the rank of the set of equations is the same. Therefore, large number of equations, m, is unnecessary if the number of nonzero singular values in the matrix $\boldsymbol{\Lambda}$ becomes n. In practice, a few number of modal flexibility matrix, N_f, and a set of equations in a single direction (either the x or y direction) are enough to reach maximum rank n. Furthermore, the choice of column in the modal flexibility matrix is arbitrary. The resulting solutions discussed in the next following section are insignificantly altered by the choice of the modal flexibility matrix if the rank of $\boldsymbol{\Lambda}$ is full.

2.6. Generalized pseudo-inverse solution using singular value decomposition

This section represents how to solve the previously derived over-determined FDIEs. The pre-multiplication of $\boldsymbol{\Lambda}^{\mathrm{T}}$ on both sides of Eq. (49) yields a reduced set of n equations:

$$\boldsymbol{\Lambda}^{\mathrm{T}}\boldsymbol{\Lambda\beta} = \boldsymbol{\Lambda}^{\mathrm{T}}\boldsymbol{\kappa}^*. \tag{50}$$

If the rank of $\boldsymbol{\Lambda}^{\mathrm{T}}\boldsymbol{\Lambda}$ is $r (r < n)$, the matrix cannot be inverted due to n–r rank deficiency. Thus the number of bases resolved in the matrix, $\boldsymbol{\Lambda}^{\mathrm{T}}\boldsymbol{\Lambda}$, is only r. The symmetric matrix, $\boldsymbol{\Lambda}^{\mathrm{T}}\boldsymbol{\Lambda}$, can be spanned by the r basis vectors $(\boldsymbol{\upsilon}_1, \boldsymbol{\upsilon}_2, \ldots, \boldsymbol{\upsilon}_r)$, because not only any column vector of $\boldsymbol{\Lambda}^{\mathrm{T}}\boldsymbol{\Lambda}$ can be spanned by its basis vector but also any row vector of $\boldsymbol{\Lambda}^{\mathrm{T}}\boldsymbol{\Lambda}$ can be spanned by the same basis due to symmetry:

$$\boldsymbol{\Lambda}^{\mathrm{T}}\boldsymbol{\Lambda} = \sigma_1\boldsymbol{\upsilon}_1\boldsymbol{\upsilon}_1^{\mathrm{T}} + \sigma_2\boldsymbol{\upsilon}_2\boldsymbol{\upsilon}_2^{\mathrm{T}} + \ldots \sigma_r\boldsymbol{\upsilon}_r\boldsymbol{\upsilon}_r^{\mathrm{T}}. \tag{51}$$

In a more convenient form, Eq. (51) can be rewritten as

$$\boldsymbol{\Lambda}^{\mathrm{T}}\boldsymbol{\Lambda} = \mathbf{Y}\boldsymbol{\Omega}\mathbf{Y}^{\mathrm{T}}, \tag{52}$$

where the $n \times r$ matrix, $\mathbf{Y} = [\,\boldsymbol{\upsilon}_1 \quad \boldsymbol{\upsilon}_2 \quad \cdots \quad \boldsymbol{\upsilon}_r\,]$, is referred to a singular vector of the matrix, $\boldsymbol{\Lambda}^{\mathrm{T}}\boldsymbol{\Lambda}$. The $r \times r$ diagonal matrix, $\boldsymbol{\Omega} = \mathrm{diag}[\,\sigma_1 \quad \sigma_2 \quad \cdots \quad \sigma_r\,]$ is referred to a singular value matrix of $\boldsymbol{\Lambda}^{\mathrm{T}}\boldsymbol{\Lambda}$. Then, the a *pseudo-inverse* solution satisfying all the Moore–Penrose conditions [17] is

$$\boldsymbol{\Gamma} = \mathbf{Y}\boldsymbol{\Omega}^{-1}\mathbf{Y}^{\mathrm{T}}. \tag{53}$$

Therefore, the desired damage index can be obtained using

$$\boldsymbol{\beta} = \mathbf{Y}\boldsymbol{\Omega}^{-1}\mathbf{Y}^{\mathrm{T}}\boldsymbol{\Lambda}^{\mathrm{T}}\boldsymbol{\kappa}^{*}. \tag{54}$$

To obtain the solution, three tasks are necessary:

(1) compute $\boldsymbol{\Lambda}^{\mathrm{T}}\boldsymbol{\Lambda}$;
(2) the singular value decomposition of $\boldsymbol{\Lambda}^{\mathrm{T}}\boldsymbol{\Lambda}$ in Eq. (52) should be performed; and
(3) the matrix multiplication in Eq. (54) should be performed.

Basically, the SVD technique for this least-squares problem gives a solution $\boldsymbol{\beta}$ that is a linear superposition of only the r eigenmatrix of $\boldsymbol{\Lambda}^{\mathrm{T}}\boldsymbol{\Lambda}$ corresponding to nonzero singular values as shown in Eq. (51). The resulting solution in Eq. (54) is a unique solution to the least-squares problem (L_2 minimization) if the $\boldsymbol{\Lambda}$ has full column rank. However, if rank of $\boldsymbol{\Lambda}$ is not full, then there are an infinite number of solutions to the least-squares problem. Let $\boldsymbol{\beta}_0$ denote a solution of Eq. (50). It is desired to show that $\boldsymbol{\beta}_0$ is an optimal solution of Eq. (50), whether or not $\boldsymbol{\Lambda}^{\mathrm{T}}\boldsymbol{\Lambda}$ can be inverted. To do this, rewrite Eq. (49) as

$$\boldsymbol{\Lambda}(\boldsymbol{\beta}_0 + \mathbf{q}) = \boldsymbol{\kappa}^{*} + \mathbf{e} \tag{55}$$

and show that the mean-squared error $\mathbf{E} = (\mathbf{e}^{\mathrm{T}}\mathbf{e})^{1/2}$ is minimized if $\mathbf{q}$ is chosen to be zero. Writing the error, $\mathbf{e} = \boldsymbol{\Lambda}(\boldsymbol{\beta}_0 + \mathbf{q}) - \boldsymbol{\kappa}^{*}$, gives

$$\mathbf{E}^2 = [\boldsymbol{\Lambda}\boldsymbol{\beta}_0 - \boldsymbol{\kappa}^{*}]^{\mathrm{T}}[\boldsymbol{\Lambda}\boldsymbol{\beta}_0 - \boldsymbol{\kappa}^{*}] + (\boldsymbol{\Lambda}\mathbf{q})^{\mathrm{T}}(\boldsymbol{\Lambda}\mathbf{q}) - 2\mathbf{q}^{\mathrm{T}}(\boldsymbol{\Lambda}^{\mathrm{T}}\boldsymbol{\Lambda}\boldsymbol{\beta}_0 - \boldsymbol{\Lambda}^{\mathrm{T}}\boldsymbol{\kappa}^{*}) \tag{56}$$

but Eq. (50) requires that the final term is exactly zero. Thus,

$$\mathbf{E}^2 = [\boldsymbol{\Lambda}\boldsymbol{\beta}_0 - \boldsymbol{\kappa}^{*}]^{\mathrm{T}}[\boldsymbol{\Lambda}\boldsymbol{\beta}_0 - \boldsymbol{\kappa}^{*}] + (\boldsymbol{\Lambda}\mathbf{q})^{\mathrm{T}}(\boldsymbol{\Lambda}\mathbf{q}). \tag{57}$$

Only the final term in Eq. (57) depends on the vector $\mathbf{q}$. Furthermore, this term is nonnegative. Thus $\mathbf{E} = (\mathbf{e}^{\mathrm{T}}\mathbf{e})^{1/2}$ is minimized by choosing $\mathbf{q} = \mathbf{0}$, showing that $\boldsymbol{\beta}_0$ is an optimal solution of Eq. (50). Therefore, the residual of this L_2 minimization is as follows:

$$\mathbf{E} = ||\boldsymbol{\Lambda}\boldsymbol{\beta}_0 - \boldsymbol{\kappa}^{*}||_2. \tag{58}$$

It is emphasized that Eq. (49) has no exact solution. An optimal approximation is the best one can do. To date, the L_2 minimization is the most feasible solution. For such a least-squares solution, the introduced *pseudo-inverse* solution using the SVD technique in Eq. (54) is numerically stable and efficient whether $\boldsymbol{\Lambda}$ has full column rank or not.

In summary, the assumptions made in the process of development of the FDIE are as follows:

(1) for a statically determinate or indeterminate linear elastic thin plate, a small damage event will have an insignificant effect on the internal forces.
(2) the mass density of a structure has not changed during the small damage event.
(3) the transverse dofs in a few of lower mode shapes before and after the small damage event are measurable through existing modal testing technique.
(4) the static deflection profile due to a unit load at the (i, j)th node is accurately approximated at the discrete measurement position using the (i, j)th modal flexibility matrix.
(5) the curvature of the measured (i, j)th modal flexibility matrix, with reasonable accuracy, can be approximated by a finite difference formula in conjunction with a *cubic Spline* interpolation.

2.7. Overall solution procedures

Based on previous results, the overall damage detection scheme can be achieved using the five steps described below.

Step 1: Using the measurements of modal parameters for the undamaged condition and the damaged condition of a structure, estimate the (i,j)th undamaged and damaged modal flexibility matrix using Eq. (3) or Eq. (4).

Step 2: Interpolate the (i,j)th modal flexibility matrix using *cubic Spline* function for coarse sensor interval.

Step 3: Using the previously interpolated deflection profiles (a set of the (i,j)th modal flexibility matrix), estimate the curvature profiles of the undamaged and the damaged structures using the central difference formula.

Step 4: Using the estimated set of curvature profiles of both the undamaged structure and the damaged structure, construct the over-determined linear matrix equation, $\mathbf{\Lambda\beta} = \boldsymbol{\kappa}^*$, (Eq. (49)).

Step 5: Use the *pseudo-inverse* technique to solve for the damage indices, $\boldsymbol{\beta}$, in Eq. (54).

3. Numerical example

In order to examine the performance of a set of two–dimensional flexural damage index equations, the simply supported plate-like structure in Fig. 4 is considered. The structure represents a model of a simply supported reinforced concrete slab bridge with the thickness of 0.15 m, the Youngs' modulus of 28.6 Gpa, the density of 2400 kg, and the Poisson's ratio of 0.15. The damage location is indicated by the gray area in Fig. 4. The simulated location of damage is

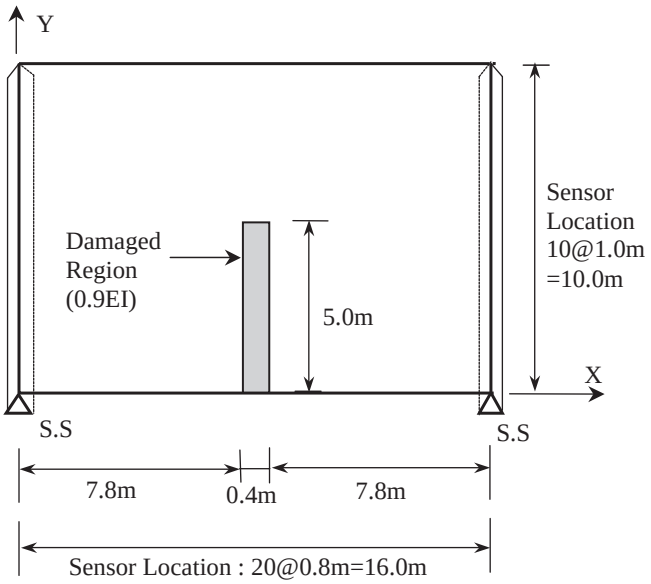

Fig. 4. Damage detection scenario of a simply supported plate.

most probable, because the live loads cause the maximum moments and deflection in such a region for the particular lane. The severity of damage is simulated by a 10% uniform reduction of Young's modulus. Thus, the exact damage index is 1.1111 in the damaged region. It is assumed that the 21×10 sensors are placed with 0.8 m and 1.0 m uniform spacing for x and y directions, respectively. Assuming that only the transverse degrees of freedom are measured at each sensor, the first six natural frequencies and displacement-normalized mode shapes are extracted for the undamaged structure and the damaged structure by means of output-only modal testing. Note that these incomplete measurement scenarios are often encountered in practice. The measured natural frequencies are shown in Table 2. It is noted that the changes in natural frequencies are insignificant due to simulated damage. The measured modes consist of the three normal bending modes and the three twisting modes. From the measured six mode shapes of the structure, modal mass for each mode is approximated by Eq. (5). For a known density of the plate, the trapezoidal integration rule is used twice for each direction after the *Cubic Spline* interpolation of 0.02 m uniform interval for both x and y directions. As shown in Table 3, the error of modal mass approximation is considered to be negligible.

In the x direction, the first six modes are the flexural modes because the plate is simply supported. However, in the y direction, the boundary condition of the plate is free at both sides. Therefore, the rigid-body modes are involved in all the measured modes except the fifth mode in the y direction. Consequently, the y direction may be inadequate for the application of the FDIE. Based on these reasons, only the x direction is considered in the following. Therefore, there are

Table 2
Natural frequency of the two span continuous plate

Mode	Undamaged (Hz)	Damaged (Hz)	Change rate (%)	Remark (Mode)
1	0.9205	0.9177	0.2977	Bending
2	2.3017	2.3006	0.0478	Twisting
3	3.6923	3.6922	0.0027	Bending
4	5.5749	5.5663	0.1543	Twisting
5	6.9955	6.9813	0.2030	Twisting
6	8.3150	8.2906	0.2934	Bending

Table 3
Modal mass approximation of the simply supported plate

Mode	Undamaged			Damaged		
	Approx. (kg)	Exact (kg)	Error (%)	Approx. (kg)	Exact (kg)	Error (%)
1	27 186	27 186	−0.0014	26 995	26 995	−0.0016
2	9964	9963	0.0108	9948	9948	0.0072
3	25 840	25 842	−0.0075	25 812	25 814	−0.0067
4	10 602	10 598	0.0346	10 569	10 566	0.0294
5	7542	7549	−0.0844	7506	7512	−0.0861
6	25 118	25 121	−0.0137	24 041	24 045	−0.0157

total nine element lanes and 10 node lanes in the y direction. Furthermore, the damage indices can be independently identified for each element lane. Using the previously estimated modal mass, a set of modal flexibility matrix due to a unit load at $x = 4$, 8, and 12 m is computed ($N_f = 3$) for each element lane. Here, the y coordinates of the unit load are dependent on the considered node lane. Recall that the location of a unit load is arbitrary. Using the *Cubic Spline* interpolation of 0.02 m uniform interval, the set of modal flexibility matrix is interpolated at $N_x = 801$ nodes in the x direction. No interpolation is conducted ($N_y = 10$) in the y direction. Then, the 800 interpolated elements can be formed for each element lanes. To identify the 800 unknowns for each element lane, only the adjacent two node lanes are necessary to construct the coupled FDIE. Thus, the number of the coupled FDIE is 1598 ($= 799 \times 2$) for one element lane for a specific modal flexibility matrix. Next, the corresponding curvature surface in the x direction is estimated using the central difference formula. Using the estimated curvature profiles for the undamaged and damaged plates, the 4794 ($= 1598 \times 3$ modal flexibilities) FDIEs are constructed to identify the 800 unknowns for each element lane. To construct the coupled FDIE in the x direction, Eqs. (47) and (48) are used to construct the over-determined linear matrix Eq. (49) for each element lane. The next involves solving the over-determined equation using the *pseudo-inverse* technique presented in Eq. (54). Identical procedures are repeated for the other element lanes. The estimated damage indices at the only sensor locations are shown in Fig. 5. The estimated damaged location can correctly be identified. Furthermore, the average value of the estimated damage indices in the damage region is $\beta = 1.1192$. Thus, it can be concluded that the flexural rigidity is reduced to 89.4% (1/1.1192) at the damaged region. It is noted that the percent error of this severity estimation is only −0.7%.

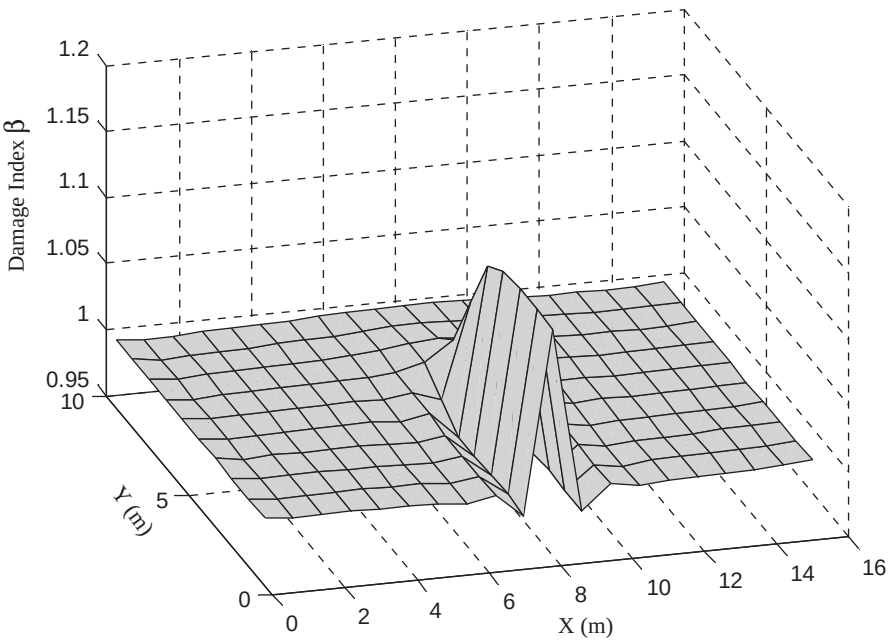

Fig. 5. Estimated damage index by the FDIE.

For the purpose of comparison study, the DI method by Choi and Stubbs [9] and the MSC method by Wahab and Roeck [7] are applied to the structure with the same damage scenario. For the DI method, the damage index for the (e,f)th element in the ith mode is defined as

$$\beta_i^{e,f} = \frac{D^{e,f}}{\bar{D}^{e,f}}, \tag{59}$$

where $D^{e,f}$ and $\bar{D}^{e,f}$ denote the flexural rigidity of the (e,f)th undamaged element and damaged element, respectively. The damage index is numerically estimated by the following:

$$\beta_i^{e,f} = \frac{\bar{f}_i^{e,f} U_i + 1}{f_i^{e,f} \bar{U}_i + 1} \tag{60}$$

with

$$f_i^{e,f} = \left(\frac{\partial^2 \phi_i}{\partial x^2} + \frac{\partial^2 \phi_i}{\partial y^2}\right)^2 - 2(1-\nu)\left[\frac{\partial^2 \phi_i}{\partial x^2}\frac{\partial^2 \phi_i}{\partial y^2} - \left(\frac{\partial^2 \phi_i}{\partial x\,\partial y}\right)^2\right]. \tag{61}$$

The modal strain energy in the ith mode, U_i, is obtained by

$$U_i = \frac{1}{2}\iint_A D f_i^{e,f}\,\mathrm{d}x\,\mathrm{d}y. \tag{62}$$

A new indicator, the normalized damage index for the ith mode, is expressed using the computed damage indices:

$$z_i^{e,f} = \frac{\beta_i^{e,f} - \mu_\beta}{\sigma_\beta}, \tag{63}$$

where μ_β and σ_β represent the mean and the standard deviation of $\beta_i^{e,f}$'s, respectively. When several modes are used, the normalized damage index obtained for each mode is superposed. Using the 0.02 m uniform interval for both x and y directions, the normalized damage index shown in Fig. 6 is numerically estimated by superposing the six mode results. The peaks near the simulated damage region are clearly identified. To estimate the severity of damage, a sensitivity algorithm that is a model-based approach can further be applied. However, unlike the proposed method, the estimation of severity of damage is not possible from the direct inspection of the estimated normalized damage index.

For the MSC method, the application to a plate is not found in technical literature yet. However, the plate considered herein can be modeled as a simple beam with a wide rectangular cross-section. Therefore, the only three bending modes (first, third, and sixth modes) are considered in the MSC method. For each mode, the absolute differences of curvature in the x direction are shown in Figs. 7–9, respectively. In the first mode, the absolute difference shows a clear peak near the damaged region. However, two peaks locate at the wrong place in the 3rd mode. The reason is that the damaged region exists at the nodal point of the third mode. This degeneracy is called the singularity problem of the MSC method. In the sixth mode, absolute curvature difference shows peaks not only at the damaged region, but also at the extremes of original mode shapes. Using this three bending modes ($n = 3$), the curvature damage factor

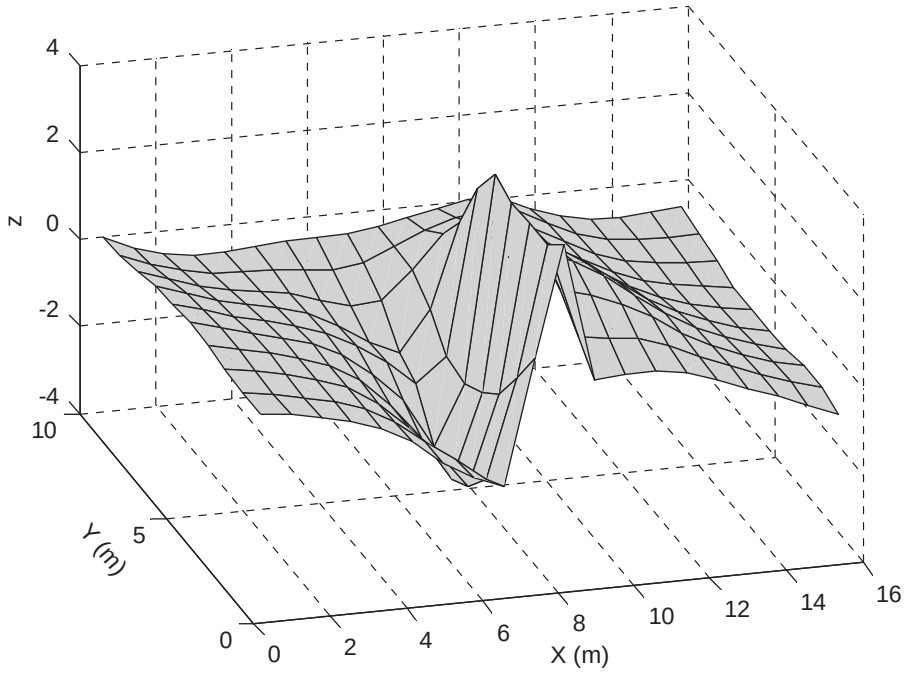

Fig. 6. Normalized damage index by the DI method.

(CDF) shown in Fig. 10 is computed by

$$\mathrm{CFD} = \frac{1}{n}\sum_{i=1}^{n}\left|\frac{\mathrm{d}^2\phi_i}{\mathrm{d}x^2} - \frac{\mathrm{d}^2\bar{\phi}_i}{\mathrm{d}x^2}\right|. \tag{64}$$

Since the absolute curvature difference in the sixth mode is dominant in magnitude, the patterns of the CDF are similar to those of Fig. 9. This result clearly shows the mode selection problem stated earlier. Although the damage detection results of the first mode are clearer than those of sixth mode, the representative damage detection results (CDF) are governed by the sixth mode. Although the MSC method successfully locates the damaged region, the severity of damage relative to the undamaged plate could not be estimated unlike the proposed method. Based on above results, it is seen that the DI method and MSC method is capable of locating damage, but the severity estimation cannot be achieved from the direct inspection of the estimated damage index. However, the proposed method is able to locate and size damage simultaneously.

To investigate the applicability of the proposed method with real conditions of measurement, two models of measurement noise are considered: one is for tilt of accelerometers caused by an inaccurate installment; the other is for random signal noise in time series. For the tilt noise, it is assumed that the accelerometers cannot be installed exactly perpendicular to the surface of the plate and their biased angles are randomly distributed from -5° to $+5^\circ$ in the y direction. The tilt noise is numerically considered by taking the cosine function for such a range of random angle

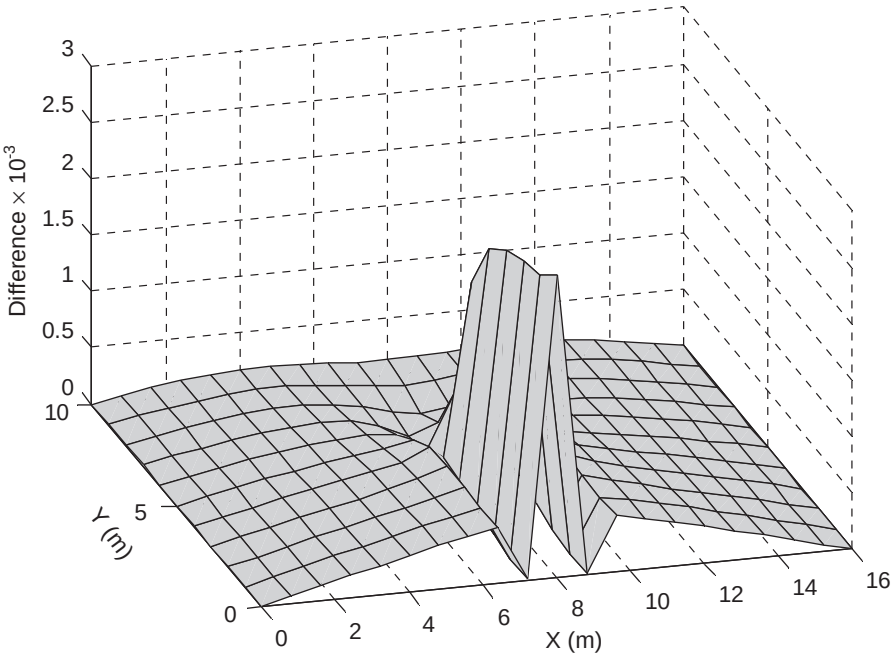

Fig. 7. Absolute curvature difference in the first mode by the MSC method.

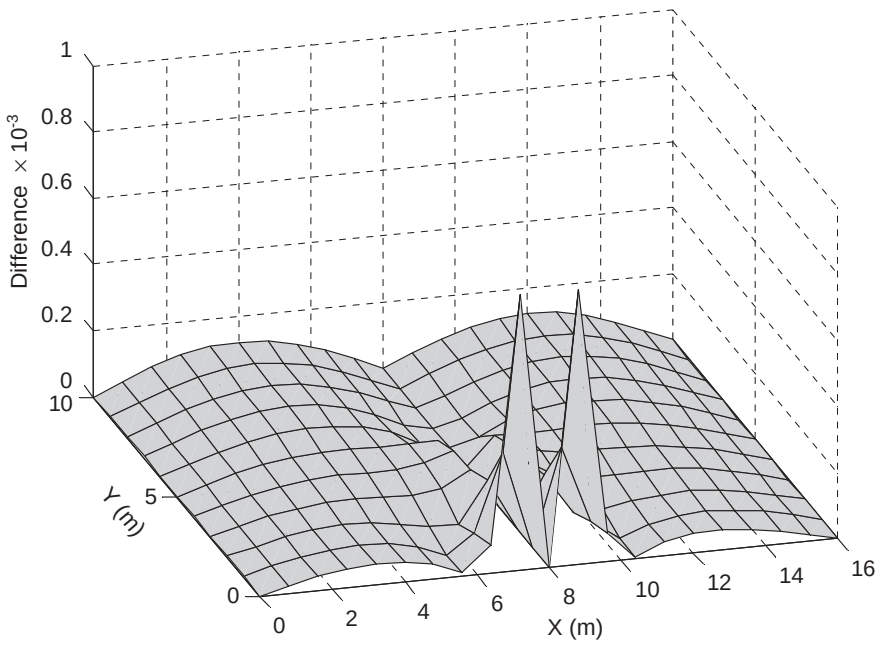

Fig. 8. Absolute curvature difference in the third mode by the MSC method.

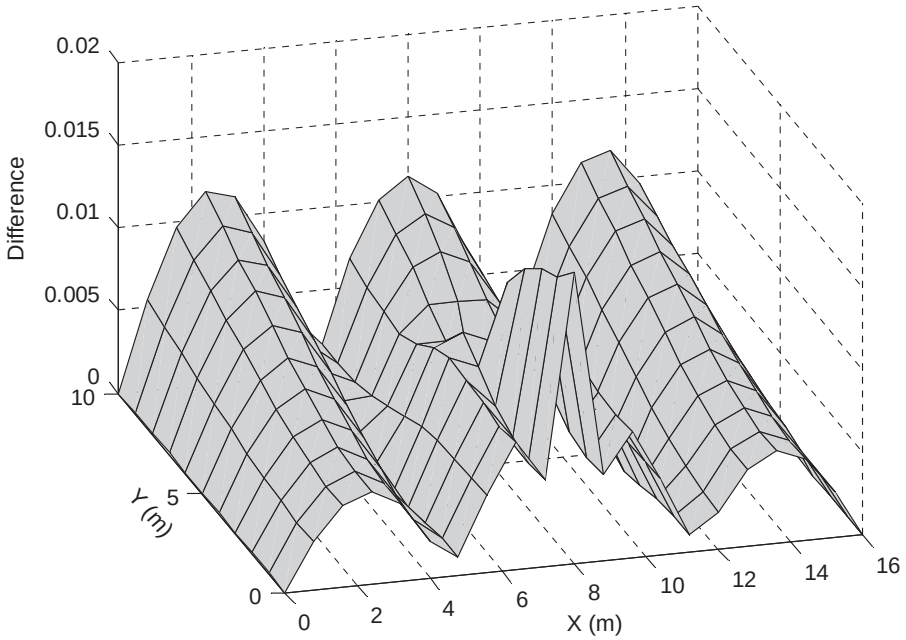

Fig. 9. Absolute curvature difference in the sixth mode by the MSC method.

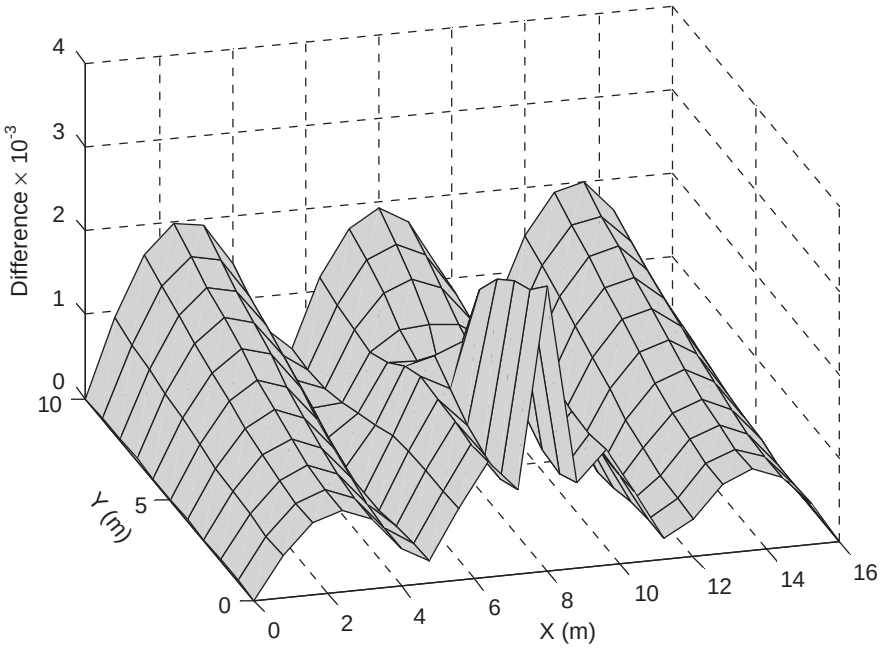

Fig. 10. Curvature damage factor by the MSC method.

and by multiplying the original mode shapes. It is also assumed that the accelerometers are not moved before and after damage. The same FDIE solution procedures are conducted, and the identified damage indices at the sensor locations are shown in Fig. 11. The location of damage is correctly identified, but the errors in the severity estimation increase to 1.76%.

The vibration-based damage detection methods commonly assume that measured modal parameters are noise-free. This requirement could be achieved by an accurate modal test and analysis with the aid of an average technique. Although modal parameter extraction is beyond the scope of this study, the sensitivity of the proposed method to random noise is simply checked out. Using the first 10 lower modes, a set of acceleration responses due to unit impulses is simulated by a state-space simulation. Here, total simulation time is 60 s and sampling frequency is 100 Hz. For each mode, a 1.5% damping ratio is used. A random noise whose maximum magnitude is 0.1% of the maximum magnitude of overall acceleration responses is added to the responses. The TDD technique, an output-only modal analysis method by Kim et al. [18], is applied to the noise-contaminated signals in order to extract the 21×10 mode shapes. For the demonstration purpose of the noise effects, the averaging process supposed to be followed in the modal analysis method is omitted. For the undamaged structure, the Modal Assurance Criterion (MAC) values between exact mode shapes and identified mode shapes are 1.0000, 1.0000, 0.9999, 0.9997, 0.9995, and 0.9997 for the first six lower modes, respectively. Using such noise-contaminated mode shapes, the same solution process is applied. As shown in Fig. 12, the identified damage indices peak near the damaged region. However, many fictitious peaks are randomly distributed due to the simulated noise. Hence, if the noise on mode shapes is serious, the peaks at the damaged region could not be distinguished from the distributed fictitious peaks.

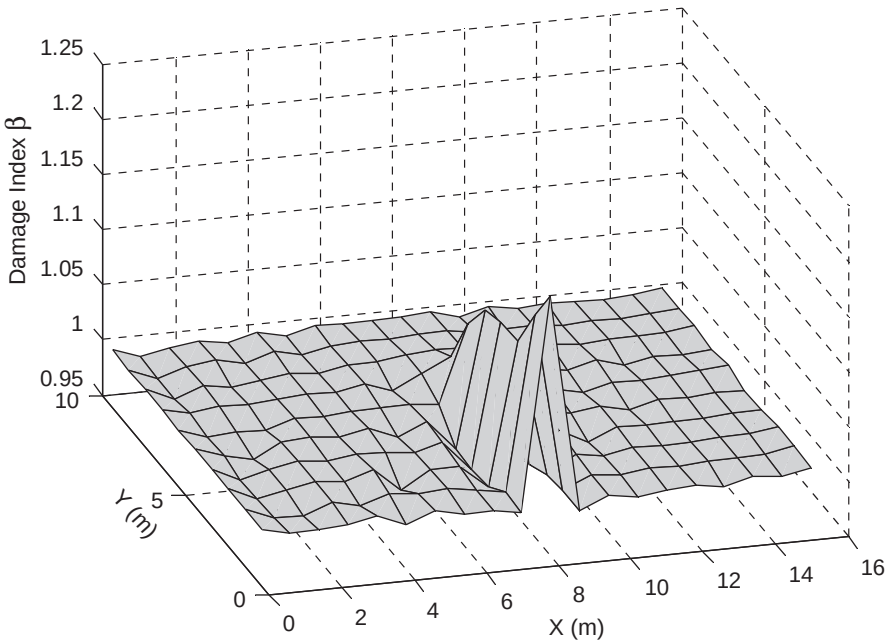

Fig. 11. Estimated damage index with tilt noise.

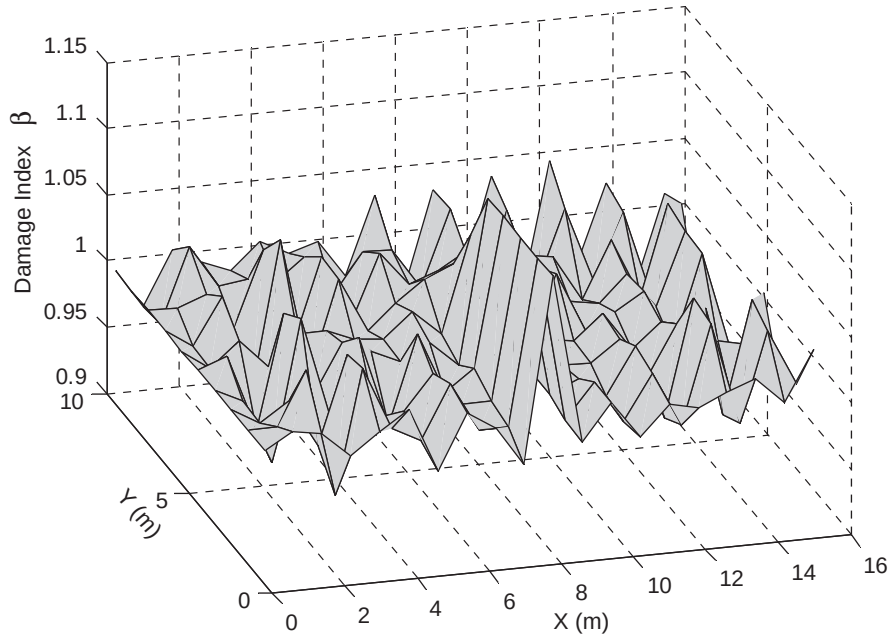

Fig. 12. Estimated damage index with random signal noise.

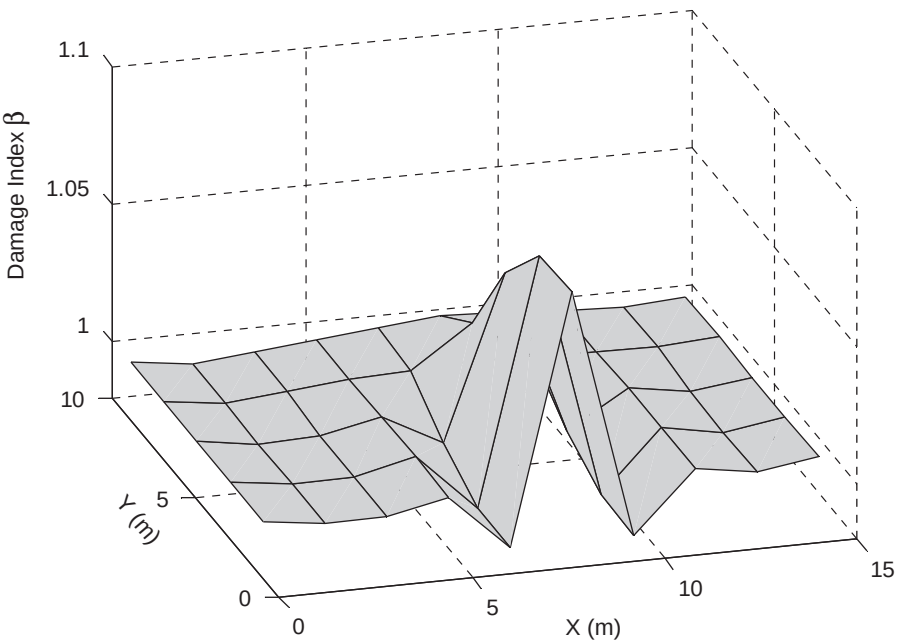

Fig. 13. Estimated damage index with a larger sensor spacing.

A detailed quantitative study for the noise sensitivity in real conditions remains as a problem to be solved.

To investigate the effect of sensor spacing, two case studies of relatively coarse sensor spacing are examined. First, the 11 × 6 sensors are placed with 1.6 m and 2.0 m uniform spacing for the x and y directions, respectively. The exact coordinates of the sensors are $x = 0$, 1.6, 3.2, 4.8, 6.4, 8.0, 9.6, 11.2, 12.8, 14.4, 16.0 m and $y = 0.0$, 2.0, 4.0, 6.0, 8.0, 10.0 m. For the same damage scenario, the identical FDIE solution procedures are repeated. The identified damage indices are illustrated in Fig. 13. Although the localization of damage is successful, the errors in the severity estimation increase to 4.2% near the damaged region. Second, the 12 × 6 sensors are placed at $x = 0.0$, 0.8, 2.4, 4.0, 5.6, 7.2, 8.8, 10.4, 12.0, 13.6, 15.2, 16.0 m and $y = 0.0$, 2.0, 4.0, 6.0, 8.0, 10.0 m. Note that all the sensors are outside of the damaged region in this case study. The identical FDIE solution procedure with the previous case study is conducted, and the resulting damage indices at the sensor locations are shown in Fig. 14. The locations of damage are clearly identifiable, but the errors in the severity estimation become worse (about 7.65%). The main reason of this degeneracy is traced to the interpolation of the measured mode shapes. For the first case of the coarse sensor spacing, the eight sensor ($x = 8.0$ m) in the x direction occasionally locates at the damaged region. This is the reason that the interpolation error of the first case is relatively smaller than those of the second case.

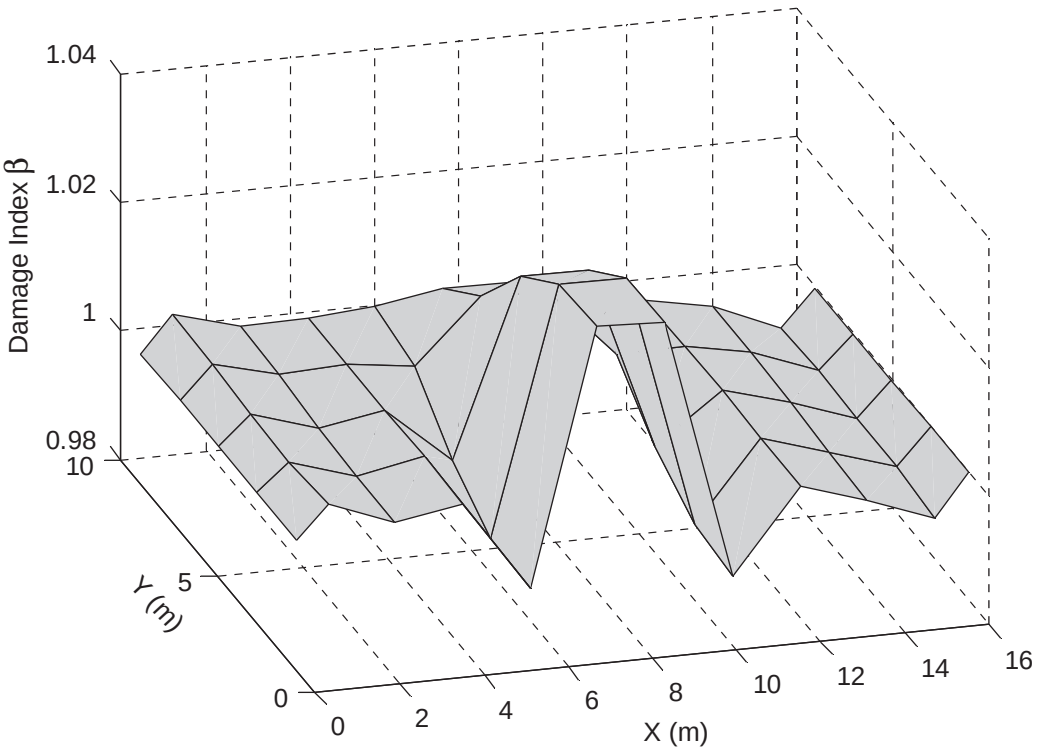

Fig. 14. Estimated damage index when sensors locate outside of the damaged region.

4. Summary and conclusions

The objective of this study is to extend the MSC method and the DI method by resolving some deficiencies of those methods. In order to achieve the goal, the small damage assumption is defined, and the FDIEs for a plate-like structure have been derived from the two-dimensional slop-deflection equations. Next, an efficient solution procedure has been introduced to solve a set of the FDIEs of a structure, and the overall procedures to localize and size damage using incomplete modal data have been summarized. Finally, the performance of the proposed method has been numerically evaluated for a simply supported plate structure with an incomplete measurement scenario.

It is emphasized that the proposed method does not suffer from the mode selection problem occurred in the MSC method and the DI method. The reason is due to the fact that the proposed method utilizes modal flexibility that is a rational way to combine modes. Furthermore, the singularity problem near the inflection points of the MSC method and the DI method is completely resolved by solving a set of linear algebraic equations, so called the FDIE. A close inspection of the derived FDIE shows that the damage and the curvature of flexibility have a strong relationship. This result is very consistent with the findings of the MSC method and the DI method.

Although the proposed technique has many features comparing to the MSC method and the DI method, there exists at least one deficiency that should be overcome near future. The proposed method requires a fine sensor interval for an accurate estimation of severity of damage. This deficiency is due to the approximation of the curvature of modal flexibility just like the MSC method and the DI method.

References

[1] A.K. Pandey, M. Biswas, M.M. Samman, Damage detection from changes in curvature mode shapes, *Journal of Sound and Vibration* 145 (2) (1991) 321–332.

[2] N. Stubbs, J.T. Kim, K. Topole, An efficient and robust algorithm for damage localization in offshore platforms, *ASCE 10th Structures Congress '92*, San Antonio, TX, 1992, pp. 543–546.

[3] C.R. Farrar, D.A. Jauregui, Comparative study of damage identification algorithms applied to a bridge: I experiment, *Smart Materials and Structures* 7 (1998) 704–719.

[4] S.W. Doebling, L.D. Peterson, K.F. Alvin, Estimation of reciprocal residual flexibility from experimental modal data, *AIAA Journal* 34 (8) (1996) 1678–1685.

[5] O.S. Salawu, C. Williams, Damage location using vibration mode shapes, *Proceedings of the 12th IMAC*, Honolulu, HI, Vol. 1, 1994, pp. 933–939.

[6] Y. Chen, A.S.J. Swamidas, Dynamic characteristic and modal parameters of a plate with a small growing surface crack, *Proceedings of the 12th IMAC*, Honolulu, HI, Vol. 2, 1994, pp. 1155–1161.

[7] M.M.A. Wahab, G.D. Roeck, Dmage detection in bridges using modal curvature, application to a real damage scenario, *Journal of Sound and Vibration* 226 (2) (1999) 217–235.

[8] N. Stubbs, J.T. Kim, C.R. Farrar, Field verification of a nondestructive damage localization and severity estimation algorithm, *Proceedings of the 13th IMAC*, Nashville, TN, Vol. 1, 1995, pp. 210–218.

[9] S. Choi, N. Stubbs, Nondestructive damage detection algorithms for 2D plates, *Smart Structures and Materials: Smart System for Bridges, Structures, and Highways SPIE Proceedings* 3043 (1997) 193–204.

[10] P. Cornwell, S.W. Doebling, C.R. Farrar, Application of the strain energy damage detection method to plate-like structures, *Journal of Sound and Vibration* 224 (2) (1999) 359–374.

[11] N. Stubbs, S. Park, C. Sikorsky, S. Choi, A global non-destructive damage assessment methodology for civil engineering structures, *International Journal of Systems Science* 31 (11) (2000) 1361–1373.
[12] T.A. Duffey, C.R. Farrar, S.W. Doebling, Damage detection for applications undergoing axial (membrane) response, *Proceedings of the 16th IMAC*, Santa Babara, CA Vol. 2, 1998, pp. 1782–1792.
[13] M.G. Srinivasan, C.A. Kot, Damage index algorithm for a circular cylindrical shell, *Journal of Sound and Vibration* 215 (3) (1998) 587–591.
[14] A. Berman, W.G. Flannelly, Theory of incomplete models of dynamic structures, *AIAA Journal* 9 (8) (1971) 1481–1487.
[15] D.J. Ewins, *Modal Testing: Theory, Practice and Application*, 2nd Ed., Research Studies Press, Hertfordshire, England, 2000.
[16] S.P. Timoshenko, J.M. Gere, *Theory of Elastic Stability*, 2nd Ed., McGraw-Hill, New York, NY, 1963.
[17] G.H. Golub, C.F. Van Loan, *Matrix Computations*, 3rd Ed., The Johns Hopkins University Press, Baltimore, MD, 1996.
[18] B.H. Kim, N. Stubbs, T. Park, A new method to extract modal parameters using output-only responses, *Journal of Sound and Vibration* 281 (1 + 2) (2005) 215–230; doi:10.1016/j.jsv.2004.02.026.